Published Online First: October, 2024
https://doi.org/10.21123/bsj.2024.9544
P-ISSN: 2078-8665 - E-ISSN: 2411-7986
Baghdad Science Journal

# Synthesis, Characterization and Biological Activity of New Ligand Derived from 4-(Dimethylamino) Benzaldehyde and Nano Copper Complex

***Enass J. Waheed***

Department of Chemistry, College of Education for Pure Sciences, Ibn -Al-Haitham, University of Baghdad, Baghdad, Iraq.

Received 19/09/2023, Revised 09/02/2024, Accepted 11/02/2024, Published Online First 20/10/2024



## Abstract

The general formula of new complexes $[M_2(BDS)Cl_4]$ are resulting from the reaction of a new ligand [N1, N4- bis (1H- benzo [d] imidazol- 2- yl) -N1, N4 -bis(4-(dimethyl amino) benzyl) succinimide] (BDS) with metal ions M(II)= Cd, Co, Hg, Cu and Ni. This ligand was derived from the reaction of the three substances 4-(Dimethyl amino) benzaldehyde, 2-amino benzimidazole, and succinyl chloride. The compounds are characterized by FT-IR, NMR, UV-Vis and Mass spectroscopy. The serine protease SplB of *Staphylococcus aureus* and the A chain of Rhomboid-protease-GLPG of *Escherichia coli* were chosen to study the binding strength of the ligand and the copper complex prepared by molecular docking method. The gold nano−$[Cu_2(BDS)Cl_4]$ was also prepared from mixing the copper complex solution with the gold nano solution, and the diagnosis was carried out using different methods, including FTIR, UV-Vis and SEM. The inhibition ability of the prepared compounds, including the nanocomplex, was tested against two types of selected bacteria (G-) *Escherichia coli* & (G+) *Staphylococcus aureus*, where the results showed that the ability of the nanocomplex to inhibit both types of bacteria was greater than the ligand and the free copper complex. The free copper complex and the nanocomplex were studied to inhibit human lung adenocarcinoma cell line (A549) and compare it with normal cell line rat embryonic fibroblasts (REF). The results showed a high ability of the nanocomplex to inhibit cancer cells, and this confirms the possibility of using it as an anticancer in the future.

**Keywords**: 4-(dimethylamino)benzaldehyde, Cell Line (A549), Gold Nano, Molecular Docking, Nanoparticles.

## Introduction

Benzimidazole derivatives are a class of organic compounds that exhibit a diverse range of biological activities, making them of significant interest in medicinal chemistry and pharmaceutical research. These compounds are characterized by a bicyclic structure consisting of a benzene ring fused to an imidazole ring, and their structural versatility allows for the development of compounds with various pharmacological properties[1].

One of the prominent biological activities associated with benzimidazole derivatives is their antimicrobial potential[2]. Benzimidazole derivatives have shown efficacy against a wide range of microorganisms, including bacteria, fungi, and parasites, making them valuable candidates for the development of antibiotics and antifungal agents[3]. Moreover, benzimidazole derivatives have demonstrated significant antitumor and anticancer activities, showing potential as chemotherapeutic agents[4].

Published Online First: October, 2024
https://doi.org/10.21123/bsj.2024.9544
P-ISSN: 2078-8665 - E-ISSN: 2411-7986
Baghdad Science Journal

These compounds have been explored for their ability to inhibit cancer cell growth and induce apoptosis, making them promising for cancer treatment[5]. Furthermore, benzimidazole derivatives exhibit anti-inflammatory properties, which can be attributed to their modulation of various pathways involved in the inflammatory response. These compounds have potential applications in the development of anti-inflammatory drugs [6]. Some benzimidazole derivatives possess significant antioxidant properties, which are essential for combating oxidative stress-related diseases as well exhibited antilytic capacity[5].

Benzimidazole derivatives have garnered significant attention in the field of medicinal chemistry and drug development. One fascinating aspect of benzimidazole derivatives is their ability to form metal complexes, leading to the emergence of a rich area of research in coordination chemistry. These metal complexes, often involving transition metals, have displayed remarkable biological activities, making them noteworthy targets for the development of novel pharmaceutical agents. Transition metal complexes of benzimidazole derivatives have demonstrated a wide range of biological activities, such as antimicrobial, antitumor, anti-inflammatory, and antioxidant properties. These compounds have been extensively studied for their potential in drug design and therapeutic applications, owing to their unique structural characteristics and the diverse reactivity of transition metal ions. For instance, the complexation of benzimidazole derivatives with metals like copper, zinc, and platinum has led to the development of promising anticancer agents due to their cytotoxic and apoptosis-inducing effects. Moreover, these metal complexes have shown significant promise as antimicrobial agents, with potential applications in the treatment of various infectious diseases[6, 7].

Nano gold, often referred to as gold nanoparticles, is a captivating and versatile class of nanomaterials that has garnered significant attention in the fields of nanotechnology and biomedical research. These minuscule gold particles, typically ranging in size from 1 to 100 nanometers, exhibit unique physicochemical properties due to their nanoscale dimensions. Their remarkable characteristics, including high surface area-to-volume ratio, tunable surface chemistry, and distinct optical properties, make them an intriguing subject of study for a wide array of applications. One of the most intriguing aspects of nano gold is its diverse range of biological activities. These activities have led to their utilization in various medical and biological contexts. Nano gold exhibits exceptional biocompatibility, which is crucial for its use in drug delivery systems, imaging techniques, and therapeutic applications. Furthermore, its distinctive plasmonic properties give rise to unique optical features, enabling their utilization in biosensing and diagnostic applications. Nano gold has also been employed in cancer therapy, gene delivery, and antimicrobial agents, showcasing its potential in addressing a variety of biomedical challenges. Notably, nano gold's biological activities are attributed to its ability to interact with biological molecules, such as proteins and nucleic acids, as well as its capacity to modulate cellular responses. These interactions have paved the way for novel therapies and diagnostic tools in the realm of nano medicine[8-10].

In this research new benzimidazole derivative was synthesized then converted to their corresponding complexes with Cd (II), Co(II) , Hg(II), Cu(II) and Ni(II). The nano gold complex was synthesized by mixing a prepared copper (II) complex solution with a nanogold solution. The complexes of benzimidazole and the nano gold complex were screened as anticancer against Cell Line (A549).

## Materials and Methods

From commercial places of certified international companies, the solvents and chemicals used in the work were purchased as they were used without purification. Using a UV-visible spectrophotometer (Shimadzu UV-1800) at a concentration of $10^{-3}$M in solvent $(CH_3)_2SO$ at (R.M) and 1.0 cm for a quartz cell length, the Uv-Vis spectra of ligand and its complexes were diagnosed. Using a spectrophotometer (Shimadzu 8400s FT-IR) of the CsI disk in the range 200-4000 $cm^{-1}$ and (Biotic. 600 FTIR) of the KBr in the range 4000 – 400 $cm^{-1}$ were determined frequencies of the active groups of the prepared compounds. Iranian university of Tabriz performed SEM. Using Bruker Avance 400 Ultra Shield NMR, originated in Germany, $^{1}$H-&$^{13}$C-NMR spectra were recorded for the bonds in DMSO-d$^{6}$. By thermogravimetric analysis (TGA), STA PT-1000 Linseis was performed in 0–700 °C as temperature limits with the use of argon (Ar) gas. By electrospray mass spectroscopy (ES) on a Shimadzu GC-Mass

Published Online First: October, 2024
https://doi.org/10.21123/bsj.2024.9544
P-ISSN: 2078-8665 - E-ISSN: 2411-7986
Baghdad Science Journal

QPA-2013 spectrometer, the mass spectrum was obtained.

**Synthesis of the New ligand [$N^1$, $N^4$- bis (1H- benzo [d] imidazol- 2- yl) -$N^1$,$N^4$-bis(4-(dimethyl amino) benzyl) Succinamide] (BDS)**

**Step1: Synthesis of (Z)- 4- (((1H- benzo [d]imidazol- 2- yl )imino)methyl)-N, N-di methyl aniline**

This compound was synthesized from procedure[11, 12]. A solution of 2-aminobenzImidazole (0.22 g, 1.68 mmol) in 10 mL absolute ethanol was added in small portions to a stirring solution of 4-(dimethylamino)benzaldehyde (0.25 g, 1.68 mmol) in 10 mL absolute ethanol with three drops of acetic acid. The mixture was heated under reflux for 4 hrs. Then it was cooled to room temperature, the precipitated was collected and washed with cold ethanol and then dried. Recrystallized by ethanol to give pale yellow precipitate.

**Step2: Synthesis of N-(4-(dimethylamino)benzyl)-1H-benzo[d]imidazol-2-amine**

This compound was synthesized according to procedure[13]. Small portions of sodium boro hydride (0.06 g, 1.68 mmol) were added to a stirring solution of compound (**Step1**) in 10 ml of tetra hydro furane: methanol (1:1). After completion, 15 mL of crushed ice add and stir the mixture vigorously for half an hour. The precipitate was collected by filtration and recrystallized after drying from aqueous methanol to give off-white crystals.

**Step3:** Synthesis **of the New Ligand (BDS)**

This compound was synthesized according to procedure[14]. A solution of (0.26 g, 0.19 mL, 1.68 mmol) Succinyl chloride in dry acetone (10 mL) was added batches to the resulting solution from Step 2 in dry acetone (10 mL) over a period of one hour. The mixture was stirred at -5°C for 14 hours, then at R.T for two hours. The formed precipitate was filtered, washed with diethyl ether, and recrystallized with ethanol. m.p. 195-197 °C (yield 83%), Scheme 1.

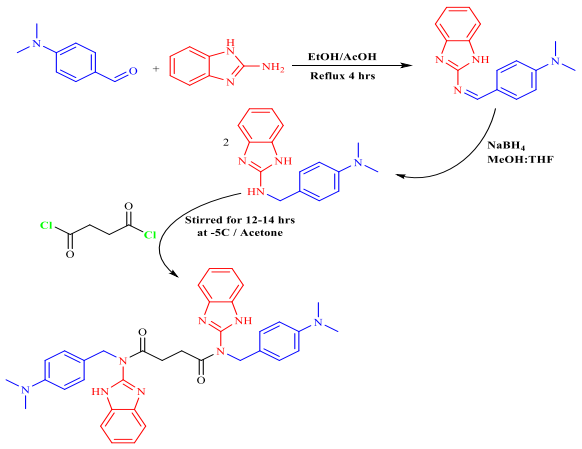


**Scheme 1. Synthesis of the ligand (BDS)**

**Synthesis of Copper Complex [$Cu_2$(BDS)$Cl_4$]**

The complex was synthesized according to procedure[15]. The molar ratio (2:1) of metal :( BDS). The metal chloride ($CuCl_2.2H_2O$) (0.6g, 3.36mmol) in (10 mL) ethanol was added to the ethanol solution (10mL) of ligand (BDS) (1g, 1.68 mmol). At 70°C, leave the mixture with continuous stirring and reflex (3-4) hours. The precipitate was filtered, washed by mix (distilled water and diethyl ether), and recrystallized by absolute ethanol; the color is bluish green. The yield % of [$Cu_2$(BDS)$Cl_4$] was 72%.

**Synthesis of [$M_2$(BDS)$Cl_4$] Complexes**

The method used to prepare [$M_2$(BDS)$Cl_4$] complexes was similar to the method mentioned in the preparation of copper complex, where M=Cd (II) , Co(II) , Hg(II) , Cu(II) and Ni(II), Fig. 1.

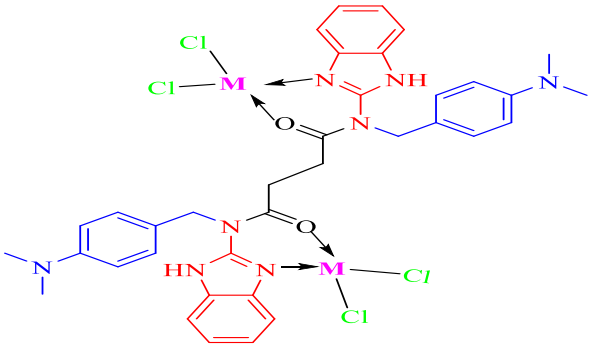

**Figure 1. Synthesis of complexes, M=Cd (II), Co (II), Hg (II), Cu (II) and Ni (II).**

**Synthesis of the Gold Nano - [$Cu_2$(BDS)$Cl_4$]**

The gold nano-[$Cu_2$(BDS)$Cl_4$] complex was synthesized according to procedure[16].This method was used to bind the nanogold with a copper complex by mixing a pre-prepared copper (II) complex solution with a nanogold solution. A two-

Published Online First: October, 2024
https://doi.org/10.21123/bsj.2024.9544
P-ISSN: 2078-8665 - E-ISSN: 2411-7986
Baghdad Science Journal

hours sonication after placing 50 mg of $[Cu_2(BDS)Cl_4]$ in 25 mL of a gold solution with a concentration of 125 mg/L was used to bind the gold nano into a complex by electrostatic force. The color of the copper complex turned blue, and after drying it showed a blue precipitation. By FTIR, SEM and UV-Vis, the nano complex was diagnosed, Scheme 2.

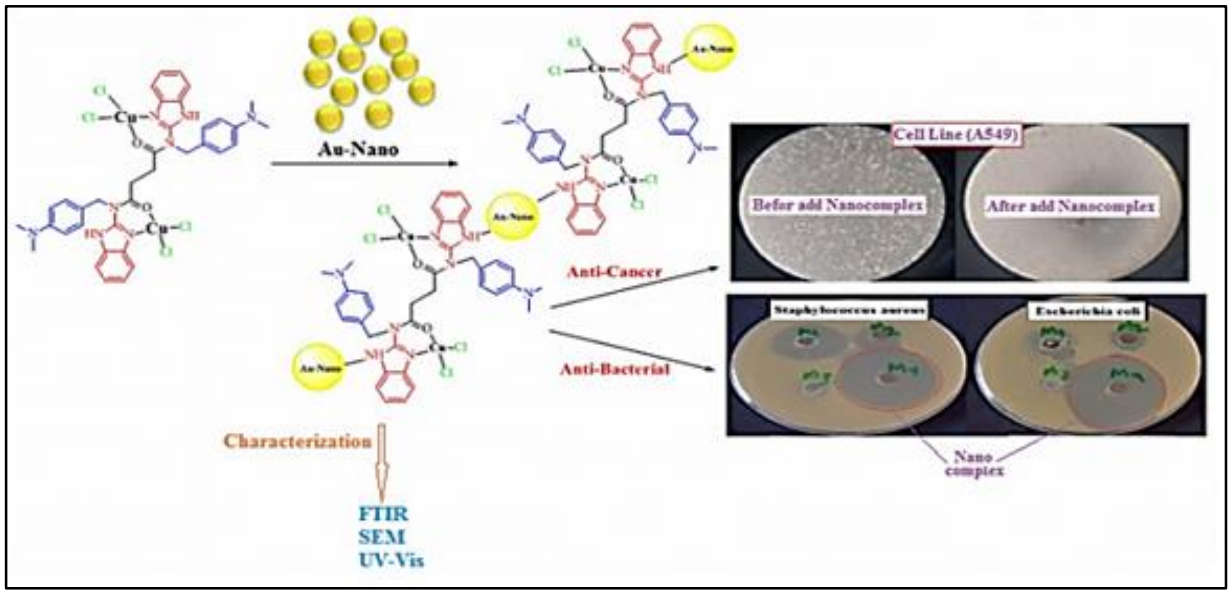


**Scheme 2. Synthesis of Gold Nano-$[Cu_2(BDS)Cl_4]$.**

## Results and Discussion

One of the most important characteristics of the prepared compounds is that they are colorful, solid, and thermally stable materials that dissolve in some organic solvents (DMSO) and (DMF), and agreat convergence was observed between their practical and theoretical results for measuring atomic absorption, as in Table 1.

**Table 1. The BDS properties and its complexes.**

| Com. | M.wt g / mol | m.p °C or dec. | Colour | Microanalysis found (calc.) % M | C | H | N | Cl |
|---|---|---|---|---|---|---|---|---|
| BDS | 614.75 | 195-197 | Off white | ------ | 70.35 (70.34) | 6.21 (6.23) | 18.22 (18.23) | ------ |
| $[Co_2(BDS)Cl_4]$ | 874.42 | 183-185 | Blue | 13.52 (13.48) | 49.44 (49.45) | 4.37 (4.38) | 12.83 (12.81) | 16.23 (16.22) |
| $[Ni_2(BDS)Cl_4]$ | 873.94 | 171-173 | Green | 13.41 (13.43) | 49.46 (49.48) | 4.36 (4.38) | 12.81 (12.82) | 16.25 (16.23) |
| $[Cu_2(BDS)Cl_4]$ | 883.65 | 215-217 | Bluish green | 14.36 (14.38) | 48.92 (48.93) | 4.34 (4.33) | 12.69 (12.68) | 16.06 (16.05) |
| $[Cd_2(BDS)Cl_4]$ | 981.99 | 188-190 | Off white | 22.92 (22.91) | 44.07 (44.06) | 3.91 (3.90) | 11.43 (11.42) | 14.46 (14.45) |
| $[Hg_2(BDS)Cl_4]$ | 1157.73 | 174-176 | Off white | 34.66 (34.65) | 37.37 (37.35) | 3.33 (3.31) | 9.67 (9.68) | 12.26 (12.25) |

**$^1$H- & $^{13}$C-NMR Spectra of ligand (BDS)**

The results $^1$H- & $^{13}$C-NMR spectra of (BDS)[17-19] listed in Table 2.

Published Online First: October, 2024
https://doi.org/10.21123/bsj.2024.9544
P-ISSN: 2078-8665 - E-ISSN: 2411-7986
Baghdad Science Journal

**Table 2. $^{1}$H-, $^{13}$C-NMR Data of BDS.**

| Ligand | Proton kids | δ (ppm) | Carbon kids | δ (ppm) |
|---|---|---|---|---|
| BDS | 4H (triplate), proton $CH_2$ group for C1 | 2.34-2.46 | C1 for ($CH_2$-$CH_2$) aliphatic in succinyl group | 29.20 ,29.63 |
| | | | C2 for C=O , amide group | 174.06 |
| | 4H (singlate), proton $CH_2$ group for C2 | 5.30 | C3 for $CH_2$, aldehyde | 56.05 |
| | | | C4 for aromatic (six ring), aldehyde | 124.76 |
| | 2H (douplate), proton aromatic (six ring) for C3 | 7.17 | C5 for aromatic (six ring), aldehyde | 127.32 |
| | | | C6 for aromatic (six ring), aldehyde | 113.41 |
| | 2H (douplate), proton aromatic (six ring) for C4 | 6.63 | C7 for aromatic (six ring), aldehyde | 151.16 |
| | | | C8 for methyl in $N(CH_3)_2$, aldehyde | 40.07-40.24 |
| | 6H (singlate), proton $CH_3$ group for C5 | 3.10 | C9 for aromatic (five ring), amine | 146.05 |
| | | | C10 for aromatic (six ring), amine | 134.40 |
| | 2H (singlate), proton NH group for C6 | 12.04 | C11 for aromatic (six ring), amine | 115.20 |
| | 8H (multiplate), proton aromatic (six ring) for C7 | 7.20-7.23 | C12 for aromatic (six ring), amine | 122.66 |

**MASS Spectra of Copper Complex [$Cu_2$(BDS)$Cl_4$]** The mass spectra fragmentation of (**BDS**)[20, 21], Scheme 3 shows ($M^+$=883.65) (18.8%) of chemical formula [$C_{36}H_{38}Cl_4Cu_2N_8O_2$] and other fragmentation.

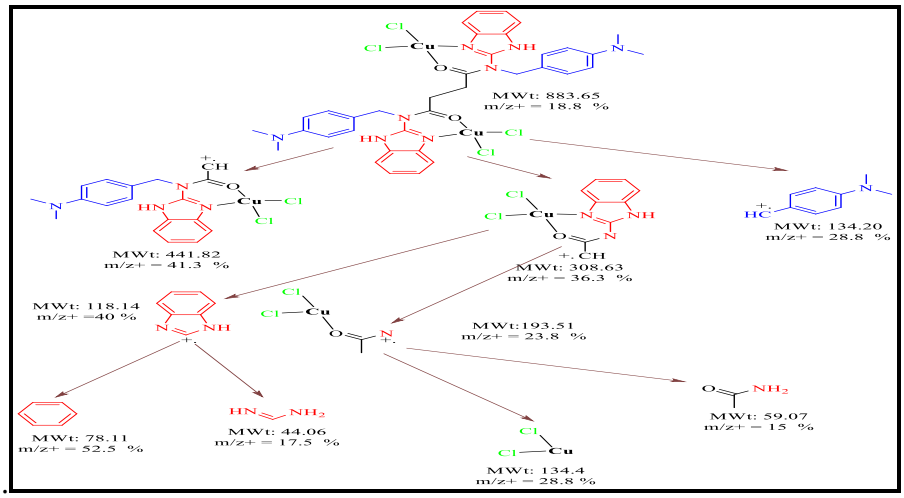


**Scheme 3. Mass Spectrum of [$Cu_2$(BDS)$Cl_4$].**

**FT-IR Spectra of Ligand (BDS) and Its Complexes** In FT-IR spectrum of (BDS), it was observed that an absorption band was recorded at 3159 $cm^{-1}$, 1679 $cm^{-1}$ and 1540 $cm^{-1}$ returning to υ(NH) $_{in\ ring}$, υ(CO) amide, and υ(C=N) $_{in\ ring}$ respectively. In FT-IR spectrum of complexes, υ($CO_{)\ amide}$ group of the complexes is noticed between 1683-1680 $cm^{-1}$ with the appearance of a new bands for υ(M-O)$_{amide}$ at the range 545-517 $cm^{-1}$, this coordination was confirmed. υ(CO) $_{amide}$ exhibit upward shift in 1679 $cm^{-1}$ after coordination to metal center which is in agreement with the υ(CO) $_{amide}$ function that coordinated to metal ion of previous reported complexes. The shift toward higher or lower frequencies is due to the interaction between the υ(CO) $_{amide}$ and metal ions. Also, there are several

Published Online First: October, 2024
https://doi.org/10.21123/bsj.2024.9544
P-ISSN: 2078-8665 - E-ISSN: 2411-7986
Baghdad Science Journal

factors that can affect the frequencies such as the metal ion nature and the coordination atoms. Moreover, bands that appear at 1569-1556 $cm^{-1}$ of ligand may be assigned to υ(C=N) $_{in\ ring}$ group. Appearance of a strong bands at the range 596-576 $cm^{-1}$ for all compounds is assignable to the υ(M-N) vibrations because of dimeric nuclear of the complex confirming the metal with υ(C=N) $_{in\ ring}$ coordination.

The bands for υ(M-Cl) at the range 370-328 $cm^{-1}$ confirm coordination of the chloride ion with the metal ion. While it was observed no shift in the absorption band for υ(N-H) $_{in\ ring}$ at the range 3160-3158 $cm^{-1}$, which confirms its in-coordination with the metal ion.

In Table 3, FT-IR spectram of the goldnano-$[Cu_2(BDS)Cl_4]$ confirmed the coordination of ligand with copper to the goldnano-$[Cu_2(BDS)Cl_4]$. The bathochromic shifts of ligand representative peaks from 3159 to 3168 $cm^{-1}$ was due to a change in the dipole moment of the goldnano complex. Hence, the copper complex was bonded to the gold nanoparticles via the nitrogen atom of ligand[9, 22, 23].

**Table 3. FT-IR data of BDS and its complexes.**

| Com. | υ(N-H) in ring | C=O)υ( Amide | (C=N)υ in ring | (M-O)υ | υ(M-N) | (M-Cl)υ |
|---|---|---|---|---|---|---|
| BDS | 3159 | 1679 | 1540 | ——— | ——— | ——— |
| $[Co_2(BDS)Cl_4]$ | 3158 | 1685 | 1556 | 594 | 524 | 335 |
| $[Ni_2(BDS)Cl_4]$ | 3159 | 1683 | 1558 | 596 | 517 | 328 |
| $[Cu_2(BDS)Cl_4]$ | 3159 | 1683 | 1569 | 581 | 532 | 363 |
| gold nano−$[Cu_2(BDS)Cl_4]$ | 3168 | 1683 | 1562 | 580 | 532 | 362 |
| $[Cd_2(BDS)Cl_4]$ | 3159 | 1685 | 1560 | 576 | 524 | 361 |
| $[Hg_2(BDS)Cl_4]$ | 3160 | 1680 | 1562 | 581 | 545 | 370 |

**UV−Vis Spectra of Ligand (BDS) and Its Complexes**

The electronic transition of the prepared ligand and its complexes[24, 25] are listed in the Table 4.

**Table 4. Electronic transfers' data of BDS and its complexes.**

| Com. | Wave number nm | Wave number $cm^{-1}$ | $\varepsilon_{max}$ molar$^{-1}$ $cm^{-1}$ | Transitions | $\mu_{eff}$ B.M. | Conducts $Ohm^1cm^2$ $mol^{-1}$ in solvent (DMSO) | geometry |
|---|---|---|---|---|---|---|---|
| BDS | 269 | 37174 | 641 | π→π* | ----- | 4.2 | --- |
| | 530 | 18867 | 602 | n→π* | | | |
| $[Co_2(BDS)Cl_4]$ | 258 | 38759 | 1993 | L . F | 4.61 | 18 | tetrahedral |
| | 341 | 29325 | 98 | C . T | | | |
| | 413 | 24213 | 124 | $^4A_2 \rightarrow {}_4T_1$ (P) | | | |
| $[Ni_2(BDS)Cl_4]$ | 269 | 37174 | 1382 | L.F | 3.83 | 17 | tetrahedral |
| | 330 | 30303 | 160 | C.T | | | |
| | 405 | 24691 | 124 | $^3T_1 \rightarrow {}^3T_1$(P) | | | |
| $[Cu_2(BDS)Cl_4]$ | 268 | 37313 | 1288 | L.F | 2.29 | 11 | tetrahedral |
| | 342 | 29239 | 88 | C.T | | | |
| | 399 | 25062 | 87 | $^2T_2 \rightarrow 2E$ | | | |
| gold nano−$[Cu_2(BDS)Cl_4]$ | 270 | 37037 | 1289 | L.F | | | tetrahedral |
| | 344 | 29069 | 87 | C.T | | | |
| | 400 | 25000 | 83 | $^2T_2 \rightarrow 2E$ | | | |
| | 550 | 18181 | 64 | goldnanocomplex | | | |
| $[Cd_2(BDS)Cl_4]$ | 266 | 37593 | 1555 | L.F | 0 | 14.8 | tetrahedral |
| | 325 | 30864 | 275 | C.T | | | |
| | 406 | 24630 | 127 | C.T | | | |
| $[Hg_2(BDS)Cl_4]$ | 260 | 38461 | 221 | L.F | 0 | 13 | tetrahedral |
| | 309 | 32362 | 86 | C.T | | | |

Published Online First: October, 2024
https://doi.org/10.21123/bsj.2024.9544
P-ISSN: 2078-8665 - E-ISSN: 2411-7986
Baghdad Science Journal

**Scanning Electron Microscope Studies (SEM)**

Surface size, morphology, crystallinity and phase locations of created material could all be researched by examining the SEM. The morphology of the surface varies for $[Cu_2(BDS)Cl_4]$ Fig. 2-A, goldnano−$[Cu_2(BDS)Cl_4]$ Fig. 2-B, that has been bound with the Au-Nano. The average size of the $[Cu_2(BDS)Cl_4]$, is ranged between 585.91-739.58 nm, while average size of the particles of goldnano−$[Cu_2(BDS)Cl_4]$ is ranged between 63.95-71.86 nm for presence of Au-Nano, gold nanoparticles have been noticed to be with the homogenous distributions on the matrix surface. The particles in nanocomposite film were found, however, some of the agglomerations of nanoparticles were also found when the surface was somewhat rough[26-28].

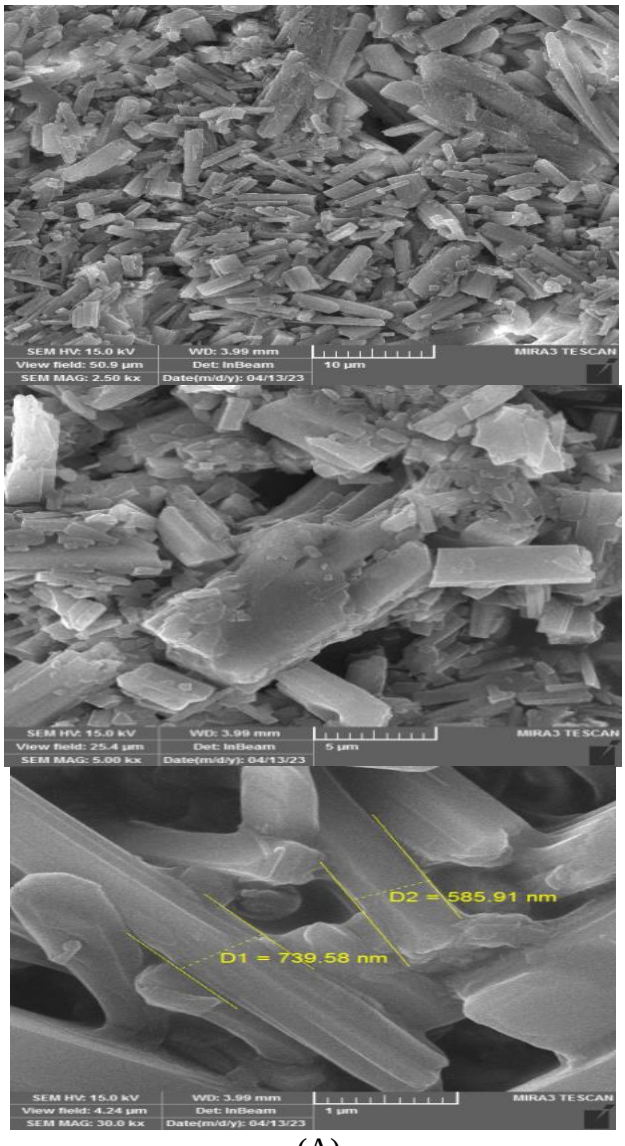


(A)

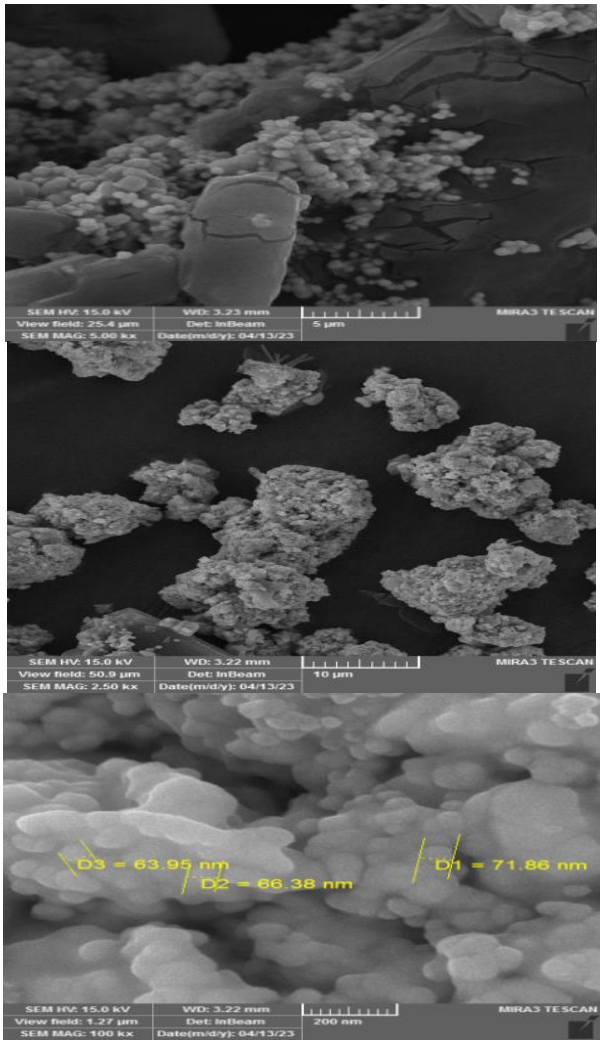


(B)

**Figure 2. SEM of free copper complex (A) and gold nano copper (B).**

**Anticancer Study**

Using cells cultured in a micro titer plate (96-well), the anticancer activity and cytotoxicity of free $[Cu_2(BDS)Cl_4]$ and gold nano-$[Cu_2(BDS)Cl_4]$ compounds at different concentrations were investigated. The test was applied through the following sequence: seeding, incubation, and finally exposure to staining. At 620 nm, the absorbance was measured on a microplate reader and by the equation below the rate of inhibition of cell growth was calculated.

$$\text{Inhibition rate} = \frac{\text{mean of control} - \text{mean of treatment}}{\text{mean of control}} \times 100$$

($IC_{50}$) (fifty inhibitor concentration), it is considered one of the most important data obtained during the assay for the inhibition of human lung cancer cell line (A549), which in turn kills almost half of the

Published Online First: October, 2024
https://doi.org/10.21123/bsj.2024.9544
P-ISSN: 2078-8665 - E-ISSN: 2411-7986
Baghdad Science Journal

cells. The $IC_{50}$ is (58.49 µg/mL) and (20.79 µg/mL) of $[Cu_2(BDS)Cl_4]$ and goldnano $-[Cu_2(BDS)Cl_4]$ respectively with the (A549) cell line. Where the results showed goldnano$-[Cu_2(BDS)Cl_4]$ compound exhibit high inhibition for cell line (A549) than $[Cu_2(BDS)Cl_4]$ complex in the lowest concentrations and the goldnano$-[Cu_2(BDS)Cl_4]$ more selective towards (A549) than the normal cells rat embryonic fibroblasts (REF) at the same time[29, 30], as the details are shown in Table 5, Fig. 3.

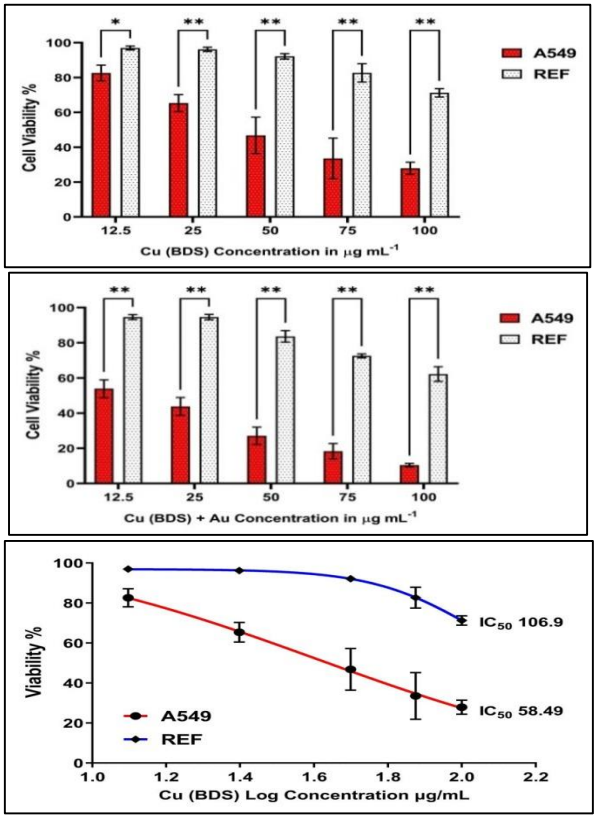


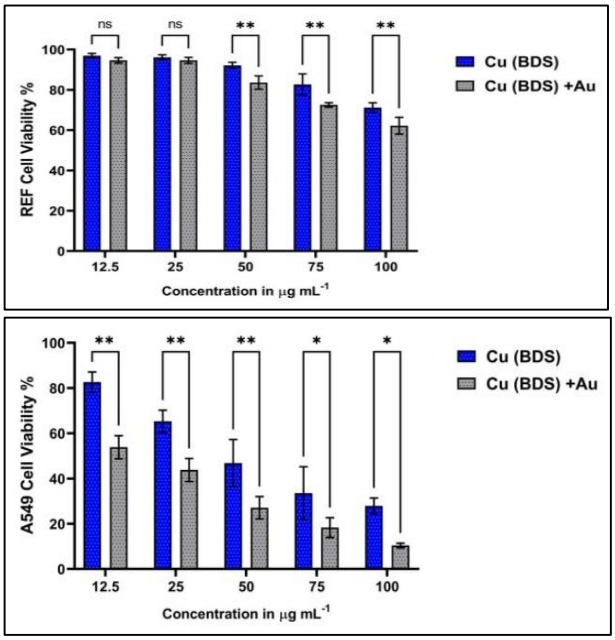


**Figure 3. The effect of the gold nano$-[Cu_2(BDS)Cl_4]$ in inhibiting cancer cells (A549).**

**Table 5. The effect of $[Cu_2(BDS)Cl_4]$ and gold nano$-[Cu_2(BDS)Cl_4]$ on (A549) and (REF).**

| Cu (BDS) | A549 | | REF | |
|---|---|---|---|---|
| Concentration | Mean | SD | Mean | SD |
| 12.5 | 82.61 | 4.54 | 96.95 | 1.14 |
| 25 | 65.36 | 4.89 | 96.18 | 1.25 |
| 50 | 46.82 | 10.43 | 92.13 | 1.56 |
| 75 | 33.55 | 11.67 | 82.70 | 5.24 |
| 100 | 27.92 | 3.49 | 71.24 | 2.37 |
| **Cu (BDS) + Au** | **A549** | | **REF** | |
| Concentration | Mean | SD | Concentration | Mean |
| 12.5 | 53.86 | 5.08 | 94.64 | 1.36 |
| 25 | 43.77 | 5.09 | 94.64 | 1.51 |
| 50 | 27.08 | 4.96 | 83.64 | 3.28 |
| 75 | 18.33 | 4.37 | 72.53 | 1.12 |
| 100 | 10.41 | 1.04 | 62.23 | 4.18 |
| **Compounds** | **Cell Line** | **$IC_{50}$ µg $mL^{-1}$** | | |
| Cu (BDS) | A549 | 58.49 | | |
| | REF | 106.9 | | |
| Cu (BDS) + Au | A549 | 20.79 | | |
| | REF | 78.29 | | |

**Biological Study**

The prepared compounds were tested against two types of bacteria (*Escherichia coli*) and (*Staphylococcus aureus*) by washing the bacterial cells in physiological saline (NaCl, 0.80%) after harvesting them by centrifugation for 5 minutes and for the purpose of inoculating the plate surface with agar, 200 µL of bacterial inoculum was spread onto

Published Online First: October, 2024
https://doi.org/10.21123/bsj.2024.9544
P-ISSN: 2078-8665 - E-ISSN: 2411-7986
Baghdad Science Journal

each agar surface and then the bacteria strains were spread in nutrient agar medium at 37 °C for 24 hrs. Next, the diluted bacteria suspension (100 µL) was collected for growth and transferred into the plate of cell. Lastly, it was incubated for 24 hrs. with shaking at 1000 revolutions per minute, after 100 µL of the compounds were added to the liquid medium, after which the inhibition diameter (mm) was measured, as the results were included in Fig. 4 and Table 6.

The ability to inhibit the bacterial activity of compounds (BDS, Cu-complex, and Nano complex) was compared, where the greatest ability to inhibition was observed at the nano complex compared with the ligand and the free Cu-complex. This is due to the larger lipophilic nature of the nano. In addition the difference in coordination or structure is where chelation tends to occur the stable nano-linking agent stronger and more effective, thus inhibiting bacterial growth. This increase in gold nano activity can be explained on the basis of chelation theory. In addition, reducing the polarity enhances the lipophilic character of the Au chelates and favors the interaction between the lipid and the Au ion, which in turn causes a breakdown of the cell permeability barrier and thus to interfere with normal cell processes and block metal binding sites in the enzymes of microorganisms[31].

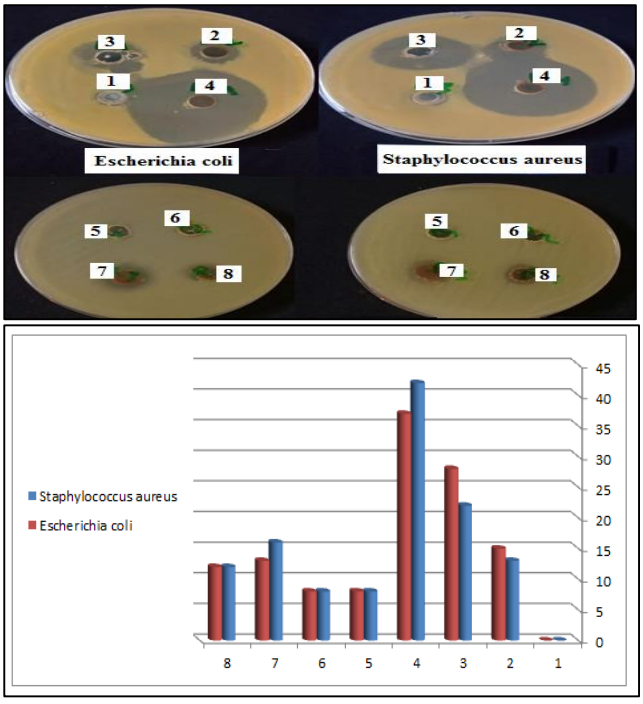


**Figure 4. Effect of prepared compounds on selected bacteria.**

**Table 6. The effect of the prepared compounds on the inhibition diameter of the selected bacteria.**

| NO | Com. | *E. coli* | *S. aureus* |
|---|---|---|---|
| 1 | DMSO | 0 | 0 |
| 2 | BDS | 15 | 13 |
| 3 | $[Cu_2(BDS)Cl_4]$ | 28 | 22 |
| 4 | gold nano−$[Cu_2(BDS)Cl_4]$ | 37 | 42 |
| 5 | $[Co_2(BDS)Cl_4]$ | 8 | 8 |
| 6 | $[Ni_2(BDS)Cl_4]$ | 8 | 8 |
| 7 | $[Cd_2(BDS)Cl_4]$ | 13 | 16 |
| 8 | $[Hg_2(BDS)Cl_4]$ | 12 | 12 |

## Thermal Study

Ligand (BDS) has been prepared as well as subjected to a thermal analysis process utilizing a STAPT-1000 device made by the German company Linseis. This measurement was carried out in an environment of argon gas at a 10°C/min heating rate with 0º–700 ºC temperature range. Any results that were reported come from the TG curves for ligand BDS that were studied[32] in Scheme. 4, Fig. 5.

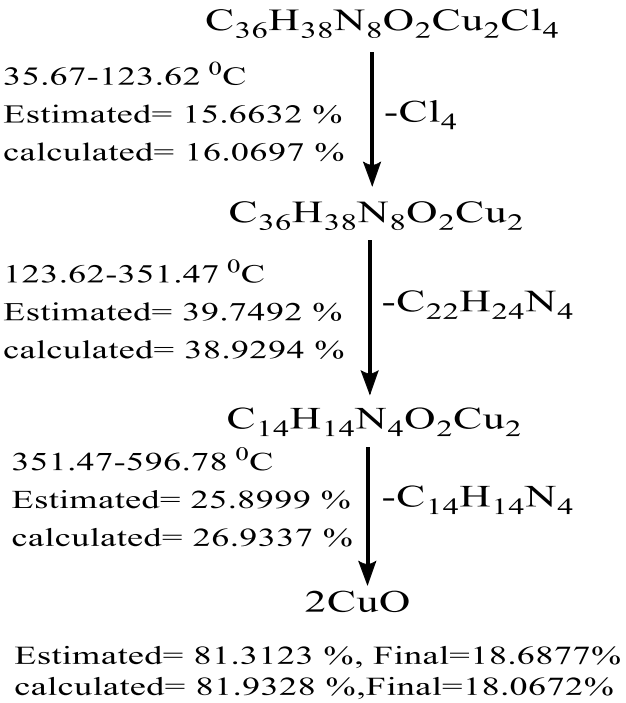


**Scheme 4. TGA fragmentation of $[Cu_2(BDS)Cl_4]$ complex.**

Published Online First: October, 2024
https://doi.org/10.21123/bsj.2024.9544
P-ISSN: 2078-8665 - E-ISSN: 2411-7986
Baghdad Science Journal

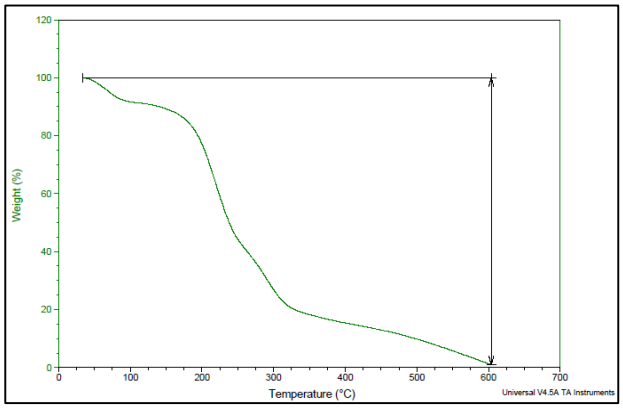


**Figure 5. Thermal data of $[Cu_2(BDS)Cl_4]$.**

**Docking Studies**

A protein (serine protease SplB) with the symbol (2vid) was selected from NCBI database https://www.ncbi.nlm.nih.gov/ of *Staphylococcus aureus* to study the binding strength of the ligand and the copper complex prepared by molecular docking method as a primary measure of the biological activity of these compounds. As for *Escherichia coli*, the A chain of Rhomboid-protease-GLPG with symbol (3zmj) in NCBI was chosen for this purpose. The application of CB-Dock[33] in carrying out the blind docking process for the prepared compounds relied on the mentioned proteins, while the use of Auto Dock Vina program was limited[34, 35] to prepare the protein molecule before the docking process.

The BDS ligand interferes with the 2vid protein on a hydrophobic pocket, the largest part of which is located on the amino acid chain {T102, P103, F104, K105, Y106, A107, A108}, which is part of the beta sheet. In addition to other segments, {N165, N166, E167, L168}, and this segment represents the beta plate as well. As for the acids {K195, I198, I202}, they overlap with the ligand as part of the alpha helix, and finally, Acids F13 and V29 they overlap with the ligand as single syllables. As mentioned , the largest area of interference between the ligand and this pocket is the hydrophobic van der Waals interferences, in addition to some charge transfer interferences, such as the transfer of charge from the $-N(CH_3)_2$ group of the ligand to the aromatic ring in F13. There is also chance of hydrogen bonding or water bridges between $-N(CH_3)_2$ at the other end of the ligand with Y106 and the pyrrole nitrogens with K105 and P103, Fig. 6-A.

The second highest degree of interference between the L3 ligand and the 2vid protein is gap No. 5 in Table 7, where the ligand is located on a group of segments, most of which are of the type of beta segment, such as {K22, S23, A24}, {H39, V40, K42, N43, Y44}, {F173, A174, S175, D176, V177}, {E153, S154, S157}, where they represent a hydrophobic pocket that works to receive the ligand through van der Waals forces and the charge transfer gap between the imidazole ring on the ligand and between the imidazole ring in H39, and water bridges and hydrogen bonds such as those between a group The carbonyl and S157, in which the proton of the hydroxyl group is the center of several hydrogen bonds, and between the imidazole proton and the carbonyl A174, Fig. 6-B.

As in the case of the BDS ligand, the complex $[Cu_2(BDS)Cl_4]$ interferes with the hydrophobic parts of the 2vid protein represented in the segments of the beta sheets {S144, S145, V147} and {Y186, G187 , V188}, {F173, A174, S175, D176}, {K75, E76, D77}, and {K38, H39} where van der Waals interferences predominate plus to the interaction of a charge transfer from the aromatic ring containing the driving group $-N(CH_3)_2$ as an electron donor group and between the aromatic ring in Y186, there is also a hydrogen bonding between the imidazole proton in the complex and the hydroxyl group K75, Fig. 6-C.

The second rank in the strength of the overlap between the $[Cu_2(BDS)Cl_4]$ complex with the 2vid protein is the gap (5), which is hydrophobic, as well as the overlap sections in it are the beta sheets {K38, H39} and {K75, E76, D77} and {F173, A174, S175, D176, V177} and {S154, S157} and the single syllable Y186 in this position represents H39 The center of strong interactions with the complex through its behavior as a receiver in the transfer of charge from the nitrogen of the amide complex. There is also a strong electrostatic interference between the nitrogen, $-N(CH_3)_3$, the methylated nitrogen, which has a positive charge, and between the carboxylates, D77, which has a charge negative, Fig. 6-D.

In BDS's overlap with the higher order 3zmj protein (gap number (1), BDS is positioned atop α helices with terminals {V236, A239, L244} and {F146}, S147, M149, H150, F153, N154} hydrophobic and retrograde turns {G246, M247, S248} and alpha helix segments {D16,M120}. The main forces in this situation, in addition to the van der Waals bonds, are the hydrogen bonding between the imidazole hydrogen in BDS and between sections G246 and M247, which hydrogen bonds with the carbonyl group in BDS, in addition to the presence of a salt bridge between the dimethyl amine group of the protonate and the carboxylate group in D116, Fig. 6-E.

Published Online First: October, 2024
https://doi.org/10.21123/bsj.2024.9544
P-ISSN: 2078-8665 - E-ISSN: 2411-7986
Baghdad Science Journal

The second place in interference strength belongs to gap (2), and it occupies almost the same position as the previous gap on segments {F146, S147, M149, H150, F153, N154}, {G246, M247, S248}, {D16, M120} and {V236, A239, L244}, and the difference here is due to the difference in the composition of the BDS complex, so the interference forces in this case are the same as in the previous case, considering the calculation taking into account the lower order of the van der Waals interferences, which made this The center ranks second, Fig. 6-F.

The first highest-ranked gap in the overlap between the $[Cu_2(BDS)Cl_4]$ complex with the 3zmj protein bearing sequence 3 in Table 7, where the overlap is attributed to a greater degree to the hydrophobic van der Waals forces, in addition to the overlaps of π-π charge transfer between its rings Aromatic substituted with the propelling dimethylamine group as a donor group and between the aromatic ring F139 as a acceptor group within a hydrophobic pocket on the surface of the protein located between the alpha helix containing the amino acid chain {L174, L175, T178,L179} and Alpha snail {F135,W136,F139}, Fig. 6-F.

The other gap, with the same overlapping forces bearing the number 5 in the Table 7, is located between the alpha helix containing the amino acids {R92, A93, W98, M101, I102, V105, F108} and the alpha helix {I151, L152 , F153, L155} It also represents a hydrophobic pocket in which van der Waals forces represent the main forces of adhesion, in addition to the charge transfer forces in this gap being more intense, such as the charge transfer of the nitrogen atom in the -N($CH_3$) group 2, and the aromatic ring of segment W98, and between the amide nitrogen in the complex and segment W159, with the presence of hydrogen bonding of the pyrrolitic proton with segment L152.

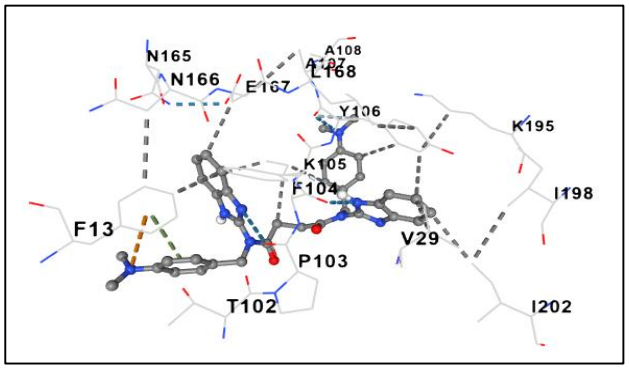


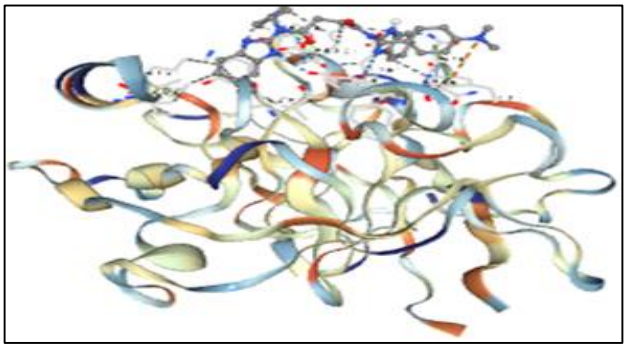

**Figure 6-A. The position of the ligand BDS overlapping with the 2vid protein, gap number 4.**

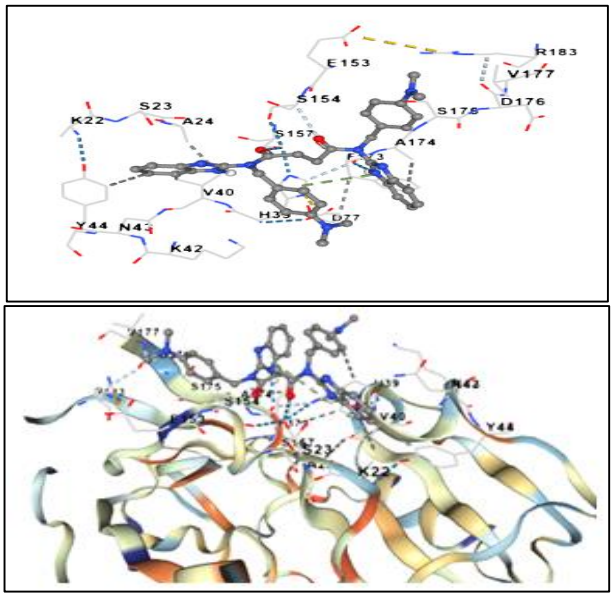


**Figure 6-B. The position of the ligand BDS overlapping with the 2vid protein, gap number 5.**

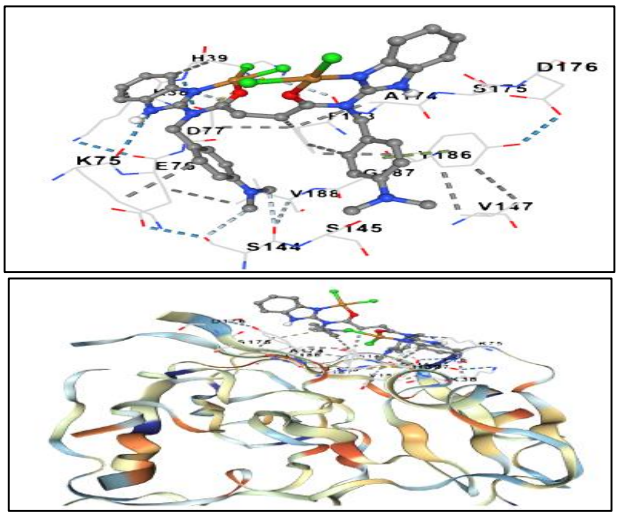


**Figure 6-C. The position of the $[Cu_2(BDS)Cl_4]$ complex overlapping with the 2vid protein, gap number 2**

Published Online First: October, 2024
https://doi.org/10.21123/bsj.2024.9544
P-ISSN: 2078-8665 - E-ISSN: 2411-7986
Baghdad Science Journal

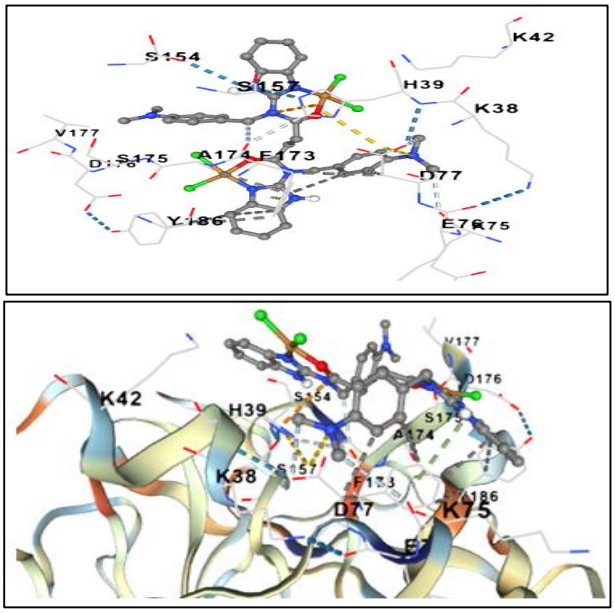


**Figure 6-D. The position of the $[Cu_2(BDS)Cl_4]$ complex overlapping with the 2vid protein, gap number 5.**

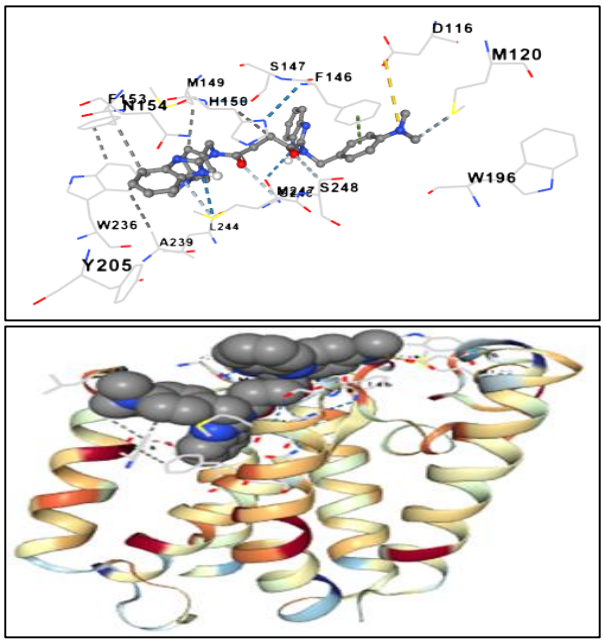


**Figure 6-E. The position of the BDS ligand overlapping with the 3zmj protein, gap number 1.**

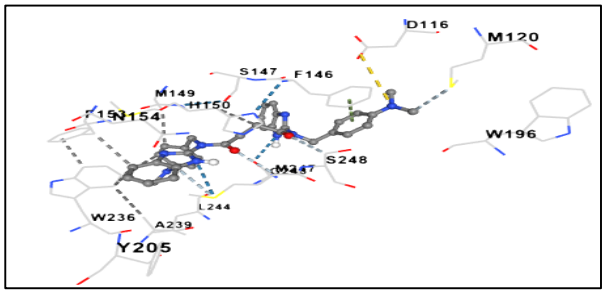


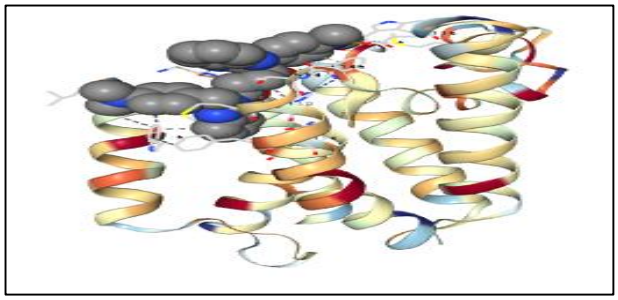

**Figure 6-F. The position of the BDS ligand overlapping with the 3zmj protein, gap number 2.**

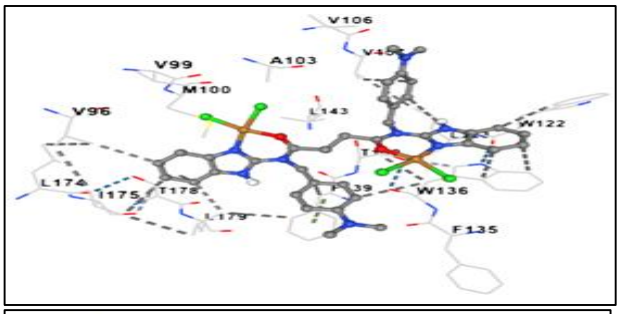


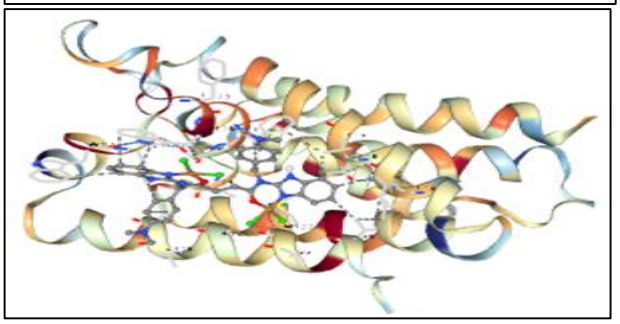

**Figure 6-G. The position of the $[Cu_2(BDS)Cl_4]$ complex overlapping with the 3zmj protein, gap number 3.**

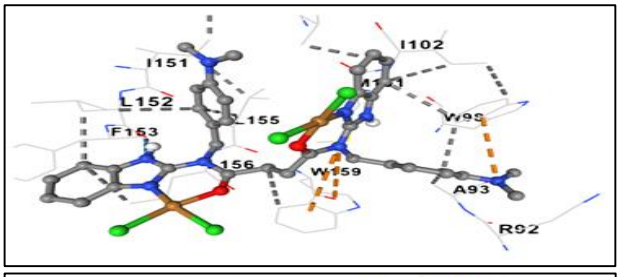


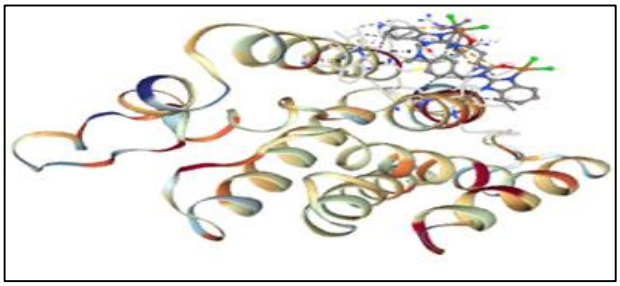

**Figure 6-H. The position of the $[Cu_2(BDS)Cl_4]$ complex overlapping with the 3zmj protein, gap number 5.**

Published Online First: October, 2024
https://doi.org/10.21123/bsj.2024.9544
P-ISSN: 2078-8665 - E-ISSN: 2411-7986
Baghdad Science Journal

**Table 7. The top five interaction modes between the studied compounds and the target proteins.**

| Cavities BDS+2vid | volume | center_x | center_y | center_z | size_x | size_y | size_z | score (kcal/mole) |
|---|---|---|---|---|---|---|---|---|
| 1 | 148 | 29.33 | 38.323 | 29.204 | 25 | 25 | 25 | -6.7 |
| 2 | 105 | 22.677 | 24.809 | 2.994 | 25 | 25 | 25 | -6.8 |
| 3 | 102 | 31.298 | 43.833 | 10.465 | 25 | 25 | 25 | -5.8 |
| 4 | 87 | 25.178 | 21.04 | 20.62 | 25 | 25 | 25 | -7.3 |
| 5 | 68 | 33.927 | 37.079 | 7.134 | 25 | 25 | 25 | -7.1 |
| **Cavities $[Cu_2(BDS)Cl_4]$+2vid** | **volume** | **center_x** | **center_y** | **center_z** | **size_x** | **size_y** | **size_z** | **score (kcal/mole)** |
| 1 | 148 | 29.33 | 38.323 | 29.204 | 26 | 26 | 26 | -6.8 |
| 2 | 105 | 22.677 | 24.809 | 2.994 | 26 | 26 | 26 | -9 |
| 3 | 102 | 31.298 | 43.833 | 10.465 | 26 | 26 | 26 | -5 |
| 4 | 87 | 25.178 | 21.04 | 20.62 | 26 | 26 | 26 | -7.1 |
| 5 | 68 | 33.927 | 37.079 | 7.134 | 26 | 26 | 26 | -7.7 |
| **Cavities BDS+3zmj** | **volume** | **center_x** | **center_y** | **center_z** | **size_x** | **size_y** | **size_z** | **score (kcal/mole)** |
| 1 | 572 | -11.371 | -7.165 | 50.643 | 25 | 25 | 25 | -9.3 |
| 2 | 191 | -9.243 | -11.579 | 56.151 | 25 | 25 | 25 | -9.2 |
| 3 | 138 | -25.209 | -2.806 | 41.799 | 25 | 25 | 25 | -6.9 |
| 4 | 104 | -8.016 | -8.238 | 30.82 | 25 | 25 | 25 | -7.5 |
| 5 | 103 | -11.125 | 5.184 | 45.728 | 25 | 25 | 25 | -7.6 |
| **Cavities $[Cu_2(BDS)Cl_4]$+3zmj** | **volume** | **center_x** | **center_y** | **center_z** | **size_x** | **size_y** | **size_z** | **score (kcal/mole)** |
| 1 | 410 | -10.158 | -7.165 | 50.643 | 26 | 26 | 26 | -8.1 |
| 2 | 191 | -9.243 | -11.579 | 56.151 | 26 | 26 | 26 | -7.6 |
| 3 | 138 | -25.209 | -2.806 | 41.799 | 26 | 26 | 26 | -9.3 |
| 4 | 104 | -8.016 | -8.238 | 30.82 | 26 | 26 | 26 | -8 |
| 5 | 103 | -11.125 | 5.184 | 45.728 | 26 | 26 | 26 | -9.3 |

**Density Functional Theory (DFT)**

Ligand (BDS) and its complex with copper $[Cu_2(BDS)Cl_4]$ were constructed by Gauss view 5 interface and performing the calculations in the Gaussian 9 program[36]. In the beginning, Geometry Optimization was done for ligand and complex according to semi-empirical Methods and the PM6 function within restricted spin conditions for ligand and unrestricted spin conditions for complex until a stable geometry is reached. An additional Geometry Optimization process was performed after changing the calculation method to unrestricted DFT with a basis function of Lanl2dz and using the Exchange Correlation Potential B3-LYP in the case of complex and restricted DFT and with a basis function of 3-21 G with the same Exchange Correlation Potential used for complex.

Upon reaching the stable geometry of the molecule, the steady-state energy was calculated according to the last calculation settings for each of the ligand and complex .

As for the geometry optimization process of the ligand (BDS) in the gas phase, it has been shown that the aromatic rings tend to approach each other in a way that tends to be somewhat parallel, which suggests the existence of a kind of π-interferences between those aromatic rings.

In the $[Cu_2(BDS)Cl_4]$ complex, it was found that the cyclic benzodiazole systems of the ligand are arranged in a planar manner with the planar squares of the coordination centers, giving the possibility of strong electronic interactions between them and the central ion in the coordination square.

The ligand (BDS) contains two types of aromatic rings, the first is the benzene ring linked to the propellant dimethyl amine group, and the other is the benzodiazole ring system, in which the effect of the diesel ring on the benzene ring fused with it has an electronic withdrawal effect, so it is not surprising to find an orbital center. HOMO in this molecule is on the aromatic ring associated with the dimethyl amine group. Therefore, the behavior of the L3 ligand as a donor to electron pairs during coordination can be done by changing the conformation position of the molecule, allowing for greater overlap between these two types of aromatic rings thus increasing the ability of the benzodiazole ring to participate as a coordination center, or through the excited state of

Published Online First: October, 2024
https://doi.org/10.21123/bsj.2024.9544
P-ISSN: 2078-8665 - E-ISSN: 2411-7986
Baghdad Science Journal

the LUMO molecule. In any case, the large spread of charge in this ligand works to reduce its polarization and thus increase its soft base characteristic compared to the ligand (BDS)[37, 38], as shown in Figs. 7-13, Table 8.

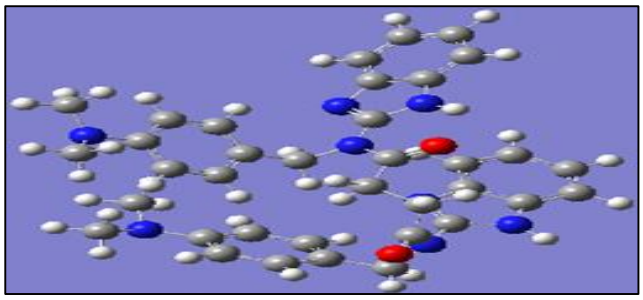

**Figure 7. Structure of ligand (BDS).**

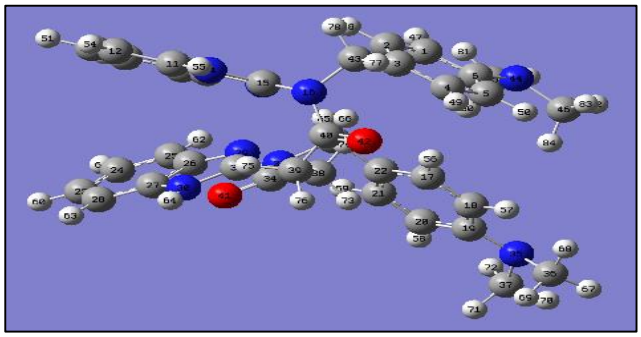

**Figure 8. Structure of the ligand (BDS) after Geometry Optimization.**

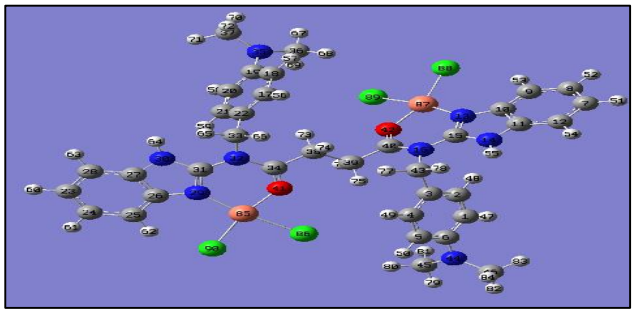

**Figure 9. The structure of the $[Cu_2(BDS)Cl_4]$ complex after Geometry Optimization.**

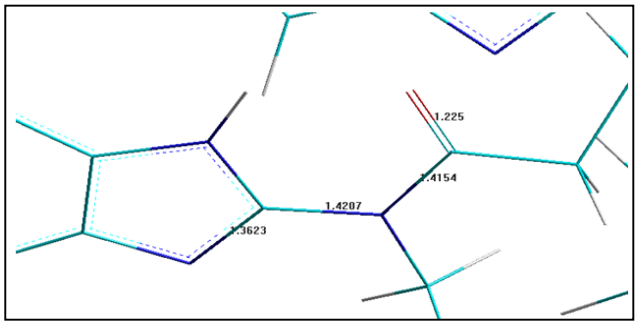


**Figure 10. The lengths of the links involved in the coordination range in the ligand (BDS).**

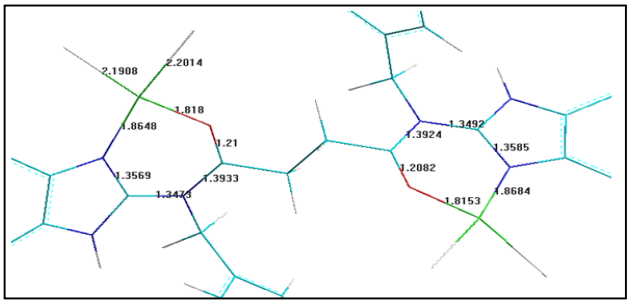


**Figure 11. The lengths of the bonds in the center of symmetry of the $[Cu_2(BDS)Cl_4]$ complex.**

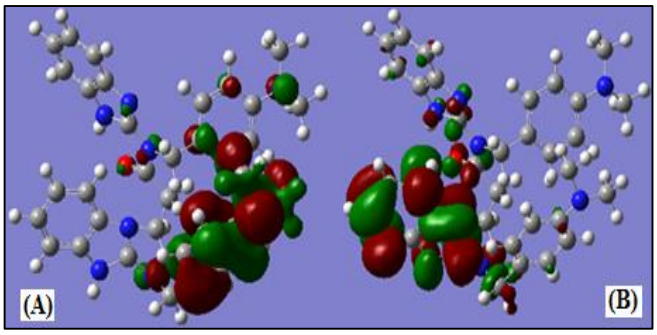


**Figure 12. The (A) HOMO and (B) LUMO energy levels of the ligand (BDS).**

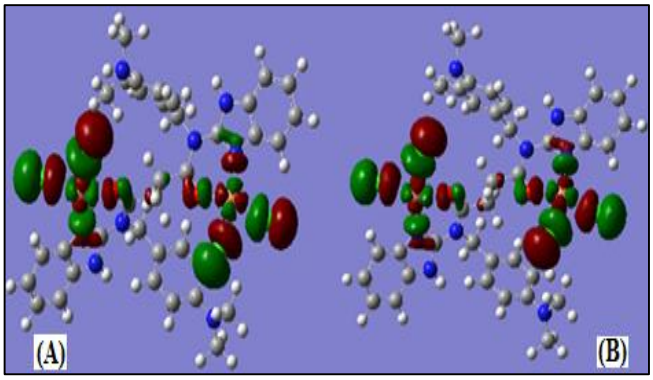


**Figure 13. HOMO (A) and (B) LUMO energy levels of $[Cu_2(BDS)Cl_4]$ complex.**

Published Online First: October, 2024
https://doi.org/10.21123/bsj.2024.9544
P-ISSN: 2078-8665 - E-ISSN: 2411-7986
Baghdad Science Journal

**Table 8. The values of the HOMO and LUMO energy levels, in addition to the functions derived from them, for each of the ligand and complex.**

| Compounds | Method | HOMO (H) | | HOMO average (H) | LUMO (H) | | LUMO average (H) |
|---|---|---|---|---|---|---|---|
| | | A | B | | A | B | |
| (BDS) | 3-21G-B3LYP | -0.187 | | -0.187 | -0.026 | | -0.026 |
| $[Cu_2(BDS)Cl_4]$ | u-lanl2dz-b3lyp | -0.152 | -0.152 | -0.152 | -0.140 | -0.140 | -0.140 |

| Compounds | Eg (energy gap)(H) | μ electronic chemical potential (H) | χ (electro-negativity) (H) | η(hardnes) (H) | σ global softness (H) | ω (electro-phlilicity index) (H) | Nu Nucleophilicity Index (H) |
|---|---|---|---|---|---|---|---|
| (BDS) | 0.160 | 0.106 | -0.106 | 0.106 | 9.396 | 0.053 | 18.792 |
| $[Cu_2(BDS)Cl_4]$ | 0.012 | 0.146 | -0.146 | 0.146 | 6.842 | 0.073 | 13.684 |

From the values of the energy levels of the orbitals HOMO and LUMO, the energy gap (Eg), the electrochemical potential (μ), the electronegativity (χ) and the hardness (η) were calculated, ductility (σ), electrophilicity criterion (ω), and nucleophilic criterion (Nu) from the following Eq. 1, 2, 3, 4, 5, 6, 7.[39-41]:

$$E_g = E_{LUMO} - E_{HOMO} \dots\dots\dots\dots 1$$

$$\mu = \frac{E_{LUMO} + E_{HOMO}}{2} \dots\dots\dots\dots 2$$

$$\chi = -\mu = \frac{-(E_{LUMO} + E_{HOMO})}{2} \dots\dots\dots\dots 3$$

$$\eta = \frac{-(E_{LUMO} - E_{HOMO})}{2} \dots\dots\dots\dots 4$$

$$\sigma = \frac{1}{\eta} \dots\dots\dots\dots\dots\dots\dots 5$$

$$\omega = \frac{\mu^2}{2\eta} \dots\dots\dots\dots\dots\dots\dots 6$$

$$Nu = \frac{1}{\omega} \dots\dots\dots\dots\dots\dots\dots 7$$

The chemical potential is a measure of the stability of the molecule, where find an increase in the stability of the complex compared to the ligand.

## Conclusion

In the present study, a newly (BDS) ligand was successfully synthesized and characterized. Moreover, five newly corresponding complexes with Cd(II), Co(II) , Hg(II) , Cu(II) and Ni(II) were successfully synthesized. The gold nano−$[Cu_2(BDS)Cl_4]$ was prepared from the mix of gold nanoparticles with the copper complex, where they were characterized by FT-IR, UV-Vis and SEM analysis. The FT-IR exhibited the bonding of gold nano with the copper complex by the (NH) in ring, gold nano results in a strong absorbance band in the visible region at 550 nm and SEM studies showed the changes in surface morphology of the synthesized complex due to the new bonds in grafted complex and gold nano. The comparison results showed that the ability of the goldnano−$[Cu_2(BDS)Cl_4]$ to inhibition was more than the free copper complex at the same concentrations. The goldnano−$[Cu_2(BDS)Cl_4]$ exhibited selective inhibition to human lung adenocarcinoma cell line death. The biological activity of nano complex showed significant inhibition ability compared to the free copper complex. The ligand molecular docking was studied and the results were discussed for the five highest interaction modes between the studied compounds and the target proteins in terms of the type of binding and binding energy.

## Acknowledgment

We would like to express our heartfelt gratitude to the personnel of the University of Baghdad for their technical support and help throughout the study period.

## Authors' Declaration

- Conflicts of Interest: None.

Published Online First: October, 2024
https://doi.org/10.21123/bsj.2024.9544
P-ISSN: 2078-8665 - E-ISSN: 2411-7986
Baghdad Science Journal

- I hereby confirm that all the Figures and Tables in the manuscript are mine. Besides, the Figures and Images, which are not mine, have been given permission for re-publication attached with the manuscript.
- No animal studies are present in the manuscript.
- No human studies are present in the manuscript.
- No potentially identified images or data are present in the manuscript.
- Ethical Clearance: The project was approved by the local ethical committee at University of Baghdad, Iraq.

## References

1. AL-Khazraji SIC, Sadik WM, Ahamed LS. Synthesis and Characterization of New 2-amino-5-chlorobenzothiazole Derivatives Containing Different Types of Heterocyclic as Antifungal Activity. Baghdad Sci J. 2023; 1(7): 1-13. https://doi.org/10.21123/bsj.2023.8318
2. Ganie AM, Dar AM, Khan FA, Dar BA. Benzimidazole derivatives as potential antimicrobial and antiulcer agents: A mini review. Mini Rev Med Chem. 2019; 19(16): 1292-1297. https://doi.org/10.2174/1381612824666181017102930
3. Šindelář Z, Kopel P. Bis (benzimidazole) Complexes, Synthesis and Their Biological Properties: A Perspective. Inorganics. 2023; 11(3): 113. http://dx.doi.org/10.3390/inorganics11030113
4. Lee YT, Tan YJ, Oon CE. Benzimidazole and its derivatives as cancer therapeutics: The potential role from traditional to precision medicine. Acta Pharm Sin B. 2023; 13(2): 478-497. https://doi.org/10.1016/j.apsb.2022.09.010
5. Moharana AK, Dash RN, Mahanandia NC, Subudhi BB. Synthesis and anti-inflammatory activity evaluation of some benzimidazole derivatives. Pharm Chem J. 2022; 56(8): 1070-1074. https://doi.org/10.1007/s11094-022-02755-3
6. Taha M, Mosaddik A, Rahim F, Ali S, Ibrahim M, Almandil NB. Synthesis, antiglycation and antioxidant potentials of benzimidazole derivatives. J King Saud Univ Sci. 2020; 32(1): 191-194. https://doi.org/10.1016/j.jksus.2018.04.003
7. Awf AR, Waheed J E, Ahmed TN. Synthesis, Characterization and Anticorrosion Studies of New Co(II), Ni(II), Cu(II), and Zn(II) Schiff Base Complexes. Int J Drug Deliv Technol. 2021; 11(2): 414-422. https://doi.org/10.1088/1742-6596/1660/1/012109
8. Suneetha G, Ayodhya D, Manjari PS. Schiff base stabilized gold nanoparticles: synthesis, characterization, catalytic reduction of nitroaromatic compounds, fluorometric sensing, and biological activities. Results Chem. 2023; 5: 100688. https://doi.org/10.1016/j.rechem.2022.100688
9. Shi L, Carn F, Boué F O, Buhler E. Gold Nanoparticle–Polyelectrolyte Complexes with Tunable Structure Probed by Synchrotron Small-Angle X-ray Scattering: Implications for the Production of Colloidal Crystals-Based Nanophotonic Materials. ACS Appl Nano Mater. 2023; 6(5): 3990-4004. https://doi.org/10.1021/acsanm.3c00259
10. Bera A, Sheet D, Paine TK. Iron (II)-α-keto acid complexes of tridentate ligands on gold nanoparticles: the effect of ligand geometry and immobilization on their dioxygen-dependent reactivity. Dalton Trans. 2023; 52(4): 1062-1073. https://doi.org/10.1039/D2DT02433K
11. Rao VK, Reddy SS, Krishna BS, Naidu KRM, Raju CN, Ghosh S. Synthesis of Schiff's bases in aqueous medium: a green alternative approach with effective mass yield and high reaction rates. Green Chem Lett Rev. 2010; 3(3): 217-223. https://doi.org/10.1080/17518251003716550
12. Shakir, RM, Saoud SA, Hussain DF, Ali KF, Algburi FS, Jasim HS. Synthesis, Antioxidant ability and Docking study for new 4, 4'-((2-(Aryl)-1H-benzo [d] imidazole-1, 3 (2H)-diyl) bis (methylene)) diphenol. Res J Chem Environ. 2022; 26(10): 10.
13. Shakir RM, Ariffin A, Ng SW. Ethyl 4-[(3, 5-di-tert-butyl-2-hydroxybenzyl) amino] benzoate. Acta Crystallogr, Sect E: Struct Rep Online. 2010; 66(11): o2916-o2916. https://doi.org/10.1107/S1600536810040742.
14. Nawras, A, Waheed, JE. Synthesis, Characterization, Thermal and Biological Study of New Organic Compound with Some Metal Complexes. Int J Drug Deliv Technol. 2021; 11(2): 401-408. http://dx.doi.org/10.25258/ijddt.11.2.30
15. Arora T, Devi J, Dubey A, Tufail A, Kumar B. Spectroscopic studies, antimicrobial activity, and computational investigations of hydrazone ligands endowed metal chelates. Appl Organomet Chem. 2023; 37(9): e7209. https://doi.org/10.1002/aoc.7209
16. Hoque A, Islam MS, Mohammad M, Khan S, Islam MM, Gazi HAR, et al. Synthesis, structural characterization of dinuclear copper (II) complexes based on Schiff base derived ligands and their impacts on DNA-binding affinities. Inorg Chim Acta. 2023; 557: 121720. https://doi.org/10.1016/j.ica.2023.121720
17. Al-Daffay RKH, Al-Hamdani AAS. Synthesis, Characterization, and Thermal Analysis of a New Acidicazo Ligand's Metal Complexes. Baghdad Sci J. 2023; 20(1): 0121-0121. https://dx.doi.org/10.21123/bsj.2022.6709

Published Online First: October, 2024
https://doi.org/10.21123/bsj.2024.9544
P-ISSN: 2078-8665 - E-ISSN: 2411-7986
Baghdad Science Journal

18. Sobornova V, Maltceva O, Khodov I, Mamardashvili NZ. $^{1}$H NMR study of kinetics of the Ni (II) and Zn (II) cations complex formation with 2-aza-5, 10, 15, 20-tetraphenyl-21-carbaporphyrin. Inorg Chim Acta. 2023; 556: 121638. https://doi.org/10.1016/j.ica.2023.121638
19. Arunadevi A, Raman N. Biological response of Schiff base metal complexes incorporating amino acids–a short review. J Coord Chem. 2020; 73(15): 2095-2116. https://doi.org/10.1080/00958972.2020.1824293
20. Al-Khazraji AMA. Synthesis of Co (ll), Ni (ll), Cu (ll), Pd (ll), and Pt (lV) Complexes with $1^{4}$, $1^{5}$, $3^{4}$, $3^{5}$-Tetrahydro-$1^{1}H$,$3^{1}H$-4,8-diaza-1,3(3,4)-ditriazola-2,6(1,4)-dibenzenacyclooctaphane-4,7-dien-$1^{5}$,$3^{5}$-dithione, and the Thermal Stability of Polyvinyl Chloride Modified Complexes. Indones J Chem. 2023; 23(3): 754-769. https://doi.org/10.22146/ijc.81272
21. Pervaiz M, Riaz A, Munir A, Saeed Z, Hussain S, Rashid A, et al. Synthesis and characterization of sulfonamide metal complexes as antimicrobial agents. J Mol Struct. 2020; 1202: 127284.https://doi.org/10.1016/j.molstruc.2019.127284
22. Al-Khazraji AM, Al Hassani R A. Synthesis, characterization and spectroscopic study of new metal complexes form heterocyclic compounds for photostability study. Sys Rev Pharm. 2020; 11(5): 535-555.https://doi.org/10.31838/srp.2020.5.71
23. Olgun U, Erdoğan E, Gülfen M, Yıldız SZ. Nano-gold-based synthesis, characterization and band gap energies of gold (III)-2 (3)-tetrakis (allyloxy)-substituted phthalocyanine and gold (III)-phthalocyanine dyes. J Mater Sci - Mater Electron. 2021; 32(11): 15011-15025. https://doi.org/10.1007/s10854-021-06054-7
24. Radwan MT, Mahmoud WH, ElMosallamy MA, El-Sherif AA. Transition metal complexes incorporating symmetric tetra dentate Schiff base ligand: Synthesis, characterization, biological activities, DFT and molecular docking studies. Egypt J Chem. 2023; 66(13): 1329-1339. http://doi.org/10.21608/EJCHEM.2023.186292.7436
25. Poryvaev AS, Yazikova AA, Polyukhov DM, Chinak OA, Richter VA, Krumkacheva OA, et al. Guest leakage from ZIF-8 particles under drug delivery conditions: quantitative characterization and guest-induced framework stabilization. J Phys Chem C. 2021; 125(28): 15606-15613. https://doi.org/10.1021/acs.jpcc.1c03876
26. Saeed RS, Attiya H G, Obead KA. Synthesis and Characterization of Grafted Chitosan Blending with Polyvinyl alcohol/Nanocomposite and Study Biological Activity. Baghdad Sci J. 2023; 20(5): 1691-1700. https://doi.org/10.21123/bsj.2023.7574
27. Mohammed HA, Ali U M, Abdullah QR. Synthesis, Characterization, Biological Activity, and Scanning Electron Microscopy Studies of Schiff Base Binuclear Complexes Co (II), Cu (II), Cd (II), and Pt (II) Derivative from Tolidine with Salicylaldehyde. Chem Methodol. 2023; 7: 594-604. http://dx.doi.org/10.22034/CHEMM.2023.397022.1678
28. Aochar RB, Mahale R, Dhivare RS. Synthesis, Physicochemical, Morphological, and Antimicrobial Study of Schiff-Base Ligands Metal Complexes. J Pharm Res. 2022; 8(2): 01-06.
29. Abdulateef S, Raypah ME, Omar A, Jafri MM, Ahmed NM, Kaus NHM, et al. Rapid synthesis of bovine serum albumin-conjugated gold nanoparticles using pulsed laser ablation and their anticancer activity on hela cells. Arabian J Chem. 2023; 16(1): 104395. https://doi.org/10.1016/j.arabjc.2022.104395
30. Minassian G, Ghanem E, El Hage R, Rahme K. Gold Nanoparticles Conjugated with Dendrigraft Poly-L-lysine and Folate-Targeted Poly (ethylene glycol) for siRNA Delivery to Prostate cancer. Nanotheranostics. 2023; 7(2): 152. http://dx.doi.org/10.7150/ntno.79050
31. Reda SM, Al-Hamdani AAS. Mn (II), Fe (III), Co (II) and Rh (III) complexes with azo ligand: Synthesis, characterization, thermal analysis and bioactivity. Baghdad Sci J. 2023; 20(3): 0642-0642. https://doi.org/10.21123/bsj.2022.7289
32. Masoud MS, Ali A E, Abd Elfatah AS, Amer G E. Synthesis, Molecular Spectroscopy, Computational, Thermal Analysis and Biological Activity of Some Orotic Acid Complexes. Open J Inorg. 2021; 11(1): 1-22. http://dx.doi.org/10.4236/ojinm.2021.111001
33. Eberhardt J, Santos-Martins D, Tillack AF, Forli S. AutoDock Vina 1.2.0: New docking methods, expanded force field, and python bindings. J Chem Inf Model. 2021; 61(8): 3891-3898. https://doi.org/10.1021/acs.jcim.1c00203
34. Liu Y, Grimm M, Dai W, Hou M, Xiao Z, Cao Y. CB-Dock: A web server for cavity detection-guided protein–ligand blind docking. Acta Pharmacol Sin. 2020; 41(1): 138-144. https://doi.org/10.1038/s41401-019-0228-6
35. Singh A, Kaushik A, Dhau JS, Kumar R. Exploring coordination preferences and biological applications of pyridyl-based organochalcogen (Se, Te) ligands. Coord Chem Rev. 2022; 450: 214-254. https://doi.org/10.1016/j.ccr.2021.214254
36. Yusuf TL, Oladipo SD, Zamisa S, Kumalo HM, Lawal IA, Lawal MM, et al. Design of new Schiff-Base Copper (II) complexes: Synthesis, crystal structures, DFT study, and binding potency toward cytochrome P450 3A4. ACS omega. 2021; 6(21): 13704-13718. https://doi.org/10.1021/acsomega.1c00906
37. Anwer KE, Hamza ZK, Ramadan RM. Synthesis, spectroscopic, DFT calculations, biological activity, SAR, and molecular docking studies of novel bioactive pyridine derivatives. Sci Rep. 2023; 13(1): 15598. https://doi.org/10.1038/s41598-023-42714-w
38. Abdou A, Abdel-Mawgoud AMM. Synthesis, structural elucidation, and density functional theory investigation of new mononuclear Fe (III), Ni (II), and

Published Online First: October, 2024
https://doi.org/10.21123/bsj.2024.9544
P-ISSN: 2078-8665 - E-ISSN: 2411-7986
Baghdad Science Journal

Cu (II) mixed-ligand complexes: Biological and catalase mimicking activity exploration. Appl Organomet Chem. 2022; 36(4): e6600. https://doi.org/10.1002/aoc.6600
39. Saracoglu M, Kandemirli F, Amin M, Vurdu CD, Cavus MS. The quantum chemical calculations of some thiazole derivatives. 3rd International Conference on Computation for Science and Technology (ICCST-3). 2015: 149-154. http://dx.doi.org/10.2991/iccst-15.2015.29
40. Farhan N, Al-Maleki AR, Ataei S, Sarih NM, Yahya R. Synthesis, DFT study, theoretical and experimental spectroscopy of fatty amides based on extra-virgin olive oil and their antibacterial activity. Bioorg Chem. 2023; 135: 106511. https://doi.org/10.1016/j.bioorg.2023.106511
41. Tzankova D, Kuteva H, Mateev E, Stefanova D, Dzhemadan A, Yordanov Y, et al. Synthesis, DFT Study, and In Vitro Evaluation of Antioxidant Properties and Cytotoxic and Cytoprotective Effects of New Hydrazones on SH-SY5Y Neuroblastoma Cell Lines. Pharmaceuticals. 2023; 16(9): 1198. https://doi.org/10.3390/ph16091198

# تحضير، تشخيص والفعالية البايولوجية لليكاند الجديد المشتق من 4-(ثنائي ميثيل أمينو) بنزالديهايد ومعقد النحاس النانوي

**ايناس جاسم وحيد**

قسم علوم الكيمياء، كلية التربية للعلوم الصرفة ،ابن الهيثم، جامعة بغداد، بغداد ، العراق.

## الخلاصة

الصيغة العامة للمعقدات الجديدة $[M_2(BDS)Cl_4]$ الناتجة من تفاعل الليكاند الجديد [ن1,ن4-ثنائي(1أ –بنزو[د] اميدازول-2-يل)-ن1,ن4-ثنائي(4-ثنائي مثيل امينو) بنزيل) سكسنمايد] (BDS) مع الايونات الفلزية الكادميوم, الكوبلت, الزئبق, النحاس والنيكل. تم اشتقاق هذا الليكاند من تفاعل المواد الثلاث 4-(ثنائي ميثيل أمينو) بنزالدهيد، 2-أمينو بنزيميدازول، وكلوريد السكسينيل. تم تشخيص المركبات باستخدام مطيافية طيف الاشعة تحت الحمراء وطيف الرنين النووي المغناطيسي وطيف الاشعة فوق البنفسجية ومطيافية الكتلة. تم اختيار بروتياز السيرين للمكورات العنقودية الذهبية وسلسلة أ من البروتياز المعيني للإشريكية القولونية لدراسة قوة ارتباط الليكاند ومعقد النحاس المحضر بطريقة الالتحام الجزيئي.

تم أيضًا تحضير معقد الذهب النانوي $[Cu_2(BDS)Cl_4]$ من مزج محلول معقد النحاس مع محلول الذهب النانوي، وتم إجراء التشخيص باستخدام طرق مختلفة، بما في ذلك طيف الاشعة تحت الحمراء وطيف الاشعة فوق البنفسجية والمجهر الإلكتروني الماسح للانبعاث. تم اختبار القدرة التثبيطية للمركبات المحضرة بما فيها معقد النحاس النانوي ضد نوعين من البكتيريا المختارة المكورات العنقودية الذهبية والإشريكية القولونية، حيث أظهرت النتائج أن قدرة معقد النحاس النانوي على تثبيط كلا النوعين من البكتيريا أكبر من الليكاند ومعقد النحاس الحر. تمت دراسة معقد النحاس الحر والمعقد النانوي لتثبيط خط خلايا سرطان الرئة الغدي البشري (A549) ومقارنته مع الخلايا الليفية الجنينية الجرذية الطبيعية (REF). وأظهرت النتائج قدرة عالية للمعقد النانوي على تثبيط الخلايا السرطانية، وهذا يؤكد إمكانية استخدامه كمضاد سرطاني في المستقبل.

**الكلمات المفتاحية:** 4-(ثنائي مثيل امينو)بنزالديهايد، خط الخلية (A549)، الذهب النانوي، الالتحام الجزيئي، الجسيمات النانوية.